UNIVERSITY OF LEEDS

This is a repository copy of *Sub-Bandgap Emission and Intraband Defect-Related Excited-State Dynamics in Colloidal $CuInS_2$/ZnS Quantum Dots Revealed by Femtosecond Pump–Dump–Probe Spectroscopy*.

White Rose Research Online URL for this paper:
http://eprints.whiterose.ac.uk/82749/

Version: Accepted Version

Article:

Kraatz, IT, Booth, M, Whitaker, BJ orcid.org/0000-0003-1554-5858 et al. (2 more authors) (2014) Sub-Bandgap Emission and Intraband Defect-Related Excited-State Dynamics in Colloidal $CuInS_2$/ZnS Quantum Dots Revealed by Femtosecond Pump–Dump–Probe Spectroscopy. Journal of Physical Chemistry C, 118 (41). pp. 24102-24109. ISSN 1932-7447

https://doi.org/10.1021/jp5065374

Reuse
Items deposited in White Rose Research Online are protected by copyright, with all rights reserved unless indicated otherwise. They may be downloaded and/or printed for private study, or other acts as permitted by national copyright laws. The publisher or other rights holders may allow further reproduction and re-use of the full text version. This is indicated by the licence information on the White Rose Research Online record for the item.

Takedown
If you consider content in White Rose Research Online to be in breach of UK law, please notify us by emailing eprints@whiterose.ac.uk including the URL of the record and the reason for the withdrawal request.

White Rose university consortium
Universities of Leeds, Sheffield & York

eprints@whiterose.ac.uk
https://eprints.whiterose.ac.uk/

Sub-Bandgap Emission and Intraband Defect-Related Excited State Dynamics in Colloidal $CuInS_2$/ZnS Quantum Dots Revealed by Femtosecond Pump-Dump-Probe Spectroscopy

Ingvar T. Kraatz,[†] Matthew Booth,[‡] Benjamin J. Whitaker,[†] Michael G.D. Nix,[†] and Kevin Critchley[‡]*

[†] School of Chemistry, [‡] School of Physics and Astronomy, University of Leeds, Leeds, LS2 9JT, United Kingdom

KEYWORDS: quantum dots, transient absorption spectroscopy, excited state dynamics, $CuInS_2$, pump-dump-probe, stimulated emission.

ABSTRACT: We consider the highly radiative, long-lived photoluminescence (PL) component observed in colloidal $CuInS_2$/ZnS core/shell quantum dots (CIS/ZnS QDs) and provide evidence of the involvement of intra-gap defect states in the emission, settling a long ongoing discussion in the literature. Femtosecond transient absorption (fs-TA) spectroscopy was used to investigate sub-picosecond dynamics in these technologically important QDs. Spectral and kinetic analysis of the fs-TA data, in combination with femtosecond pump-dump-probe (PDP) experiments, revealed a stimulated emission (SE) component in CIS/ZnS QDs for the first time. PDP experiments showed that the excited state absorption (ESA) signal, originating from the conduction band (CB), was immune to the depopulation of

the emitting state by a third, ‘dump’ laser centered close to the luminescence maximum. We conclude that the optical transition responsible for the observed room-temperature PL in CIS/ZnS QDs cannot originate from the CB as postulated in the literature, but rather from high-lying intraband donor states most likely associated with indium-copper anti-site defects. Filling of the emitting sub-bandgap state was assigned with a time constant of 0.5 ps and de-excitation via remaining surface states was associated with a 1.8 ps time constant. A third longer decay constant (27 ps) was attributed to Auger recombination.

Introduction

The inherent bond length mismatch ($R_{I\text{-}VI} \neq R_{III\text{-}VI}$) in ternary I-III-$VI_2$ chalcopyrite semiconductor compounds such as $CuInS_2$ (CIS) is manifested as an anion displacement,[1-3] leading to a tetragonal distortion of the crystal lattice and an abundance of intrinsic point-defects.[4] These structural perturbations strongly influence the optoelectronic properties of such materials and render this group of semiconductors widely applicable. Generally, the band gaps of I-III-VI_2 materials are anomalously reduced relative to the band gaps of their binary II-VI analogues[5] and either *n*-type or *p*-type behaviour can be selected by tuning the off-stoichiometry without introducing external impurities.[6] Furthermore, the band gaps are stable against off-stoichiometry (due to a dynamic interplay between the band edge positions and defect formation energies).[7-9]

The band gap of bulk CIS (1.53 eV)[10] is such that CIS quantum dots (CIS QDs) can be size-tuned to optimally absorb within the solar spectrum and to emit in the red to near-infra-red region of the spectrum. These QDs have thus been advocated for use, amongst other applications, as the absorbing components in photovoltaic solar cells and as fluorescent probes for the imaging of biological systems,[11, 12] because they are expected to have a reduced toxicity compared to Cd-based QDs.[13, 14]

An elegant synthesis route towards highly crystalline, luminescent CIS QDs has been established and CIS QDs coated with a CdS or ZnS shell (*i.e.* CIS/CdS or CIS/ZnS QDs) have enhanced photoluminescence quantum yield (PLQY) compared to the core-only CIS QDs, approaching that of Cd-based QDs.[15] It is clear that the binary Zn or Cd sulfide layer saturates the 'dangling' bonds at the QD surfaces, effectively removing surface defects and non-radiative intra-gap trap states associated with them.[16-18] Despite this understanding, the mechanism behind the radiative component observed in CIS QDs (and more dramatically in CIS/ZnS QDs) remains unclear, with various models of exciton recombination having been suggested in the literature.[15, 19, 20]

A better understanding of the excited state dynamics in CIS QDs is required before the system can be optimized for a particular application. In the context of the broad potential applications an improved understanding of exciton recombination dynamics will enable more efficient charge extraction techniques to be developed for solar cells based on CIS QDs, and in biological imaging applications will enable the penetration of the emission through biological samples to be maximized, reducing the QD dose required.

Several studies have investigated the highly luminescent and long-lived nature of the emission from CIS QDs, primarily by means of PL spectroscopy.[15, 19-26] Surprisingly, CIS QDs show a large Stokes-shift and the emission band is very broad. This is in contrast to the characteristic small Stokes-shift and narrow emission band observed for 'band-edge' emission in CdSe QDs.[16, 17] The emission characteristics of CIS QDs suggest that the PL dynamics involve deep intra-gap defect states. This is supported by two further observations: firstly, that for large CIS nanoparticles the 'red' side of the PL spectral peak extends to longer wavelengths (> 850 nm) than a band edge transition in the bulk material would permit. Secondly, the PLQY of Cu-poor CIS QDs, which is expected to have a high density of defects associated with copper vacancies, is greater than that of an equivalent stoichiometric sample.[27, 28] It has been frequently suggested that this defect-related emission originates from donor-acceptor pair (DAP) recombination, although various trap states and mechanisms have been invoked.[19, 20, 23, 28-32]

A coupling from the CB to the emitting donor state is necessary for DAP recombination to occur and either a radiative or non-radiative transfer of energy is required. Time-resolved (nanosecond) PL spectroscopy performed on CIS and CIS/ZnS QDs have identified a highly radiative component with a long lifetime (on the order of 100 ns) which is enhanced upon ZnS shell formation, whilst a faster component associated with surface trap states is suppressed.[15, 33] These studies conclude that the emission upon excitation is instantaneous (on the nanosecond timescale) and therefore originates from the CB, which partially contradicts the DAP recombination postulated by Nam *et al.*[19] Nevertheless, population transfer

between the CB to a donor state could be possible on an ultra-fast time-scale, reconcilable with fast moving electrons and 'electron deficient' donor states.

A first attempt to gain information about possible ultra-fast non-radiative contributions in the relaxation process in CIS/CdS QDs following photo-excitation was undertaken by Li *et al*.[15] in the form of fs-TA spectroscopy. A loss feature was observed at the band edge position after 4 ps and was attributed to the bleaching of the ground state (GSB). However no contribution from SE or ESA was identified. Furthermore, no time-dependent fs-TA data were presented.

In the present study the ultra-fast exciton relaxation dynamics over the first 50 ps in CIS/ZnS QDs are probed by fs-TA spectroscopy, in an attempt to observe SE and the GSB recovery. TA spectroscopy holds many advantages over steady-state absorption spectroscopy and even time-resolved PL spectroscopy, since both the electron and hole dynamics can be resolved. The results are discussed in the context of two recent publications by Sun *et.al*[34] and Cadirci *et.al*[35] that also investigated the dynamics with fs-TA spectroscopy. We employ Gaussian fitting in the spectral domain to reveal that the negative TA signal is composed of two components (GSB and SE) and perform pump-dump-probe (PDP) experiments in order to directly observe the depopulation of the emitting state. The results are contradictory to previous suggestions that the emission originates from the CB, rather than a sub-bandgap state as our data implies.

Experimental Section

***Materials*:** Indium (III) acetate (99.99 %), copper (I) iodide (99.999 %), dodecanethiol (DDT, > 98 %), zinc stearate (90 %), and octadecene (ODE, 90 %) were purchased from Sigma Aldrich. HPLC grade methanol, chloroform, acetone and hexane (> 97 %) were purchased from Fisher Scientific (UK). All chemicals were used as received.

Synthesis of CIS/ZnS QDs: CIS QDs were synthesized following methods reported elsewhere.[36] Briefly, 0.1 mmol of copper (I) iodide, 0.1 mmol of indium (III) acetate and 4 ml of DDT were placed in

a three-neck flask which was then purged with argon for 30 minutes before being heated to 100 °C, whilst being continuously stirred. After ten minutes, the powders were fully dissolved in the DDT and the solution had turned a transparent yellow colour. The solution temperature was raised to 210 °C under argon. The temperature was maintained for a set period of time (*i.e.* 5-60 minutes) and then rapidly cooled, the reflux time governing the size of the nanocrystals. In this case, the reflux time was set at 10 minutes to produce ~ 3 nm QDs. The ZnS shell was formed on the CIS NPs by introducing 0.2 mmol of zinc stearate, dissolved in 4 ml of ODE, to the as-synthesized NP solution. The temperature of the solution was raised back to 220 °C and maintained for 60 minutes.

Nanoparticle cleaning: The CIS/ZnS/DDT QDs in hexane were diluted tenfold in a chloroform/methanol/acetone mixture (1:1:10). The solution was then centrifuged at 4000 rpm for 10 minutes at room temperature, resulting in a QD pellet. The supernatant was decanted and the QDs were re-suspended in hexane. The cleaning process was cycled at least three times. The hydrophobic QDs were stored at 8 °C protected from light.

Spectrophotometry and spectrofluorophotometry: UV-Visible absorption spectra were recorded with a Perkin−Elmer Model Lambda900 spectrophotometer. Photoluminescence spectra were recorded with a Jobin Yvon Horiba FluoroMax-3 fluorescence spectrometer fitted with a red-sensitive detector calibrated to the manufacturer's standard. The excitation wavelength was set to 540 nm.

Transient absorption and pump-dump-probe spectroscopy: The transient absorption experiments were conducted with a Ti:sapphire laser system (CPA2110, Clark-MXR Inc.). The fundamental (772 nm with an output power of 1 W at a repetition rate of 1 kHz with temporal full width half-maximum (FWHM) of 150 fs) was split into three separate beam lines to generate a tuneable pump pulse, the probe continuum and the dump pulse.

The pump pulse was generated by converting a part of the 772 nm fundamental in a commercially available nonlinear optical parametric amplifier (TOPAS-white, Light Conversion Ltd.) to yield tunable

pulses in the range 500 nm to 650 nm. The pump pulses were near the transform limit with temporal FWHM < 60 fs, as measured by frequency-resolved optical gating, and all experiments were conducted with average pump energy of < 1.2 μJ and a spot size of ~100 μm at the sample, giving a fluence of approximately 10 mJ cm^{-2}. Reflective focusing optics were used to minimize chromatic and temporal aberrations.

The probe continuum was generated by focusing an IR-beam centered at 1060 nm into a 1 cm fused silica cuvette filled with deionized water, with convection heating. The IR pulse was generated in a commercially available nonlinear optical parametric amplifier (NOPA, Clark-MXR Inc.) with an energy output of approximately 8 μJ. The white light stability was improved with a long-pass filter (RG850) to remove the CPA fundamental and a variable neutral density filter to attenuate the pulse energy prior to the white light generation. The temporal chirp of the probe continuum was corrected mathematically in data processing, by determining the initial chirp function on basis of the experimentally observed coherence spike and thus allowing for the correction of each probe wavelength to time zero.

A fraction (1-4 μJ) of the fundamental 772 nm laser pulse served as an alternative pump pulse and was also used as dump pulse in the three-pulse PDP experiments.

The sample stage used a 0.5 mm fused silica flow cell with a micro-pump (M400K, TCS Micropumps Ltd.). The flow rate was sufficiently high to replace the excited volume between laser shots at the 1 kHz laser repetition rate.

Detection of the white light continuum was achieved using a diode array detector with 1024 deep well pixels (LW-ELIS-1024A-1394, ISG of NY Inc.), after dispersion in a prism based home-built spectrometer. The pump light was chopped at 500 Hz to yield signal and background measurements on consecutive shots. These were subsequently divided to produce TA data in software (LABView). The pump-probe time delay was controlled with femtosecond resolution using a digitally controlled motorised delay stage (IMS600CCHA, Newport Spectra-Physics Ltd.)

Results and Discussion

The PL and UV/Vis absorption spectra of the CIS/ZnS QDs are consistent with literature[15, 25] and are shown in Figure 1. As expected, the formation of a ZnS shell significantly enhances the PL intensity (not shown) and slightly blue-shifts the emission, as reported elsewhere.[36] The UV/Vis data of both core and core/shell samples are spectrally almost identical, showing absorption out to about 700 nm. The second derivative of the CIS/ZnS QDs data indicates that the first excitonic transition is centred at approximately 540 nm. Upon excitation at this wavelength the steady-state PL spectrum shows a single broadband emission centred at 693 nm with FWHM approximately 100 nm. Based on an empirically determined relationship[36] between the length of the triangular projection of CIS QDs in TEM images and their PL spectral peak position, the height of the pyramid of the QD cores was estimated to be 3.4 nm.

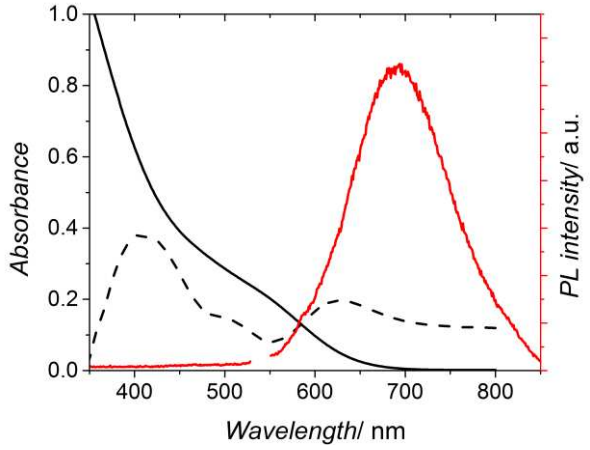

Figure 1. UV/Vis (black line) and PL (red line) spectra of CIS/ZnS QDs dispersed in hexane. The dashed line shows the second derivative of the absorption spectrum, revealing the first band centre at ~540 nm.

Transient Absorption Spectroscopy

Figure 2 shows the spectral transient absorption data as a function of time delay (Δt). The change in optical density (ΔOD) is calculated according to the formula

$$\Delta OD(\lambda,\Delta t) = -\log\left(\frac{I(\lambda,\Delta t)_{Pump\ ON}}{I(\lambda,\Delta t)_{Pump\ OFF}}\right)$$

wherein $I(\lambda,\Delta t)_{PumpON}$ and $I(\lambda,\Delta t)_{PumpOFF}$ represents the absorption spectra at each time delay with the pump switched on and off, respectively. The strong loss in optical density ($\Delta OD < 0$) between 550 nm and 700 nm must correspond to a reduction in absorption or a gain due to stimulated emission. This band aligns with the first excitonic feature seen in figure 1, and indicates a GSB (that slowly recovers over the first 20 ps). A significant, but rapidly decaying positive signal ($\Delta OD > 0$) is observed within 5 ps at longer and shorter wavelengths, and is associated with ESA.

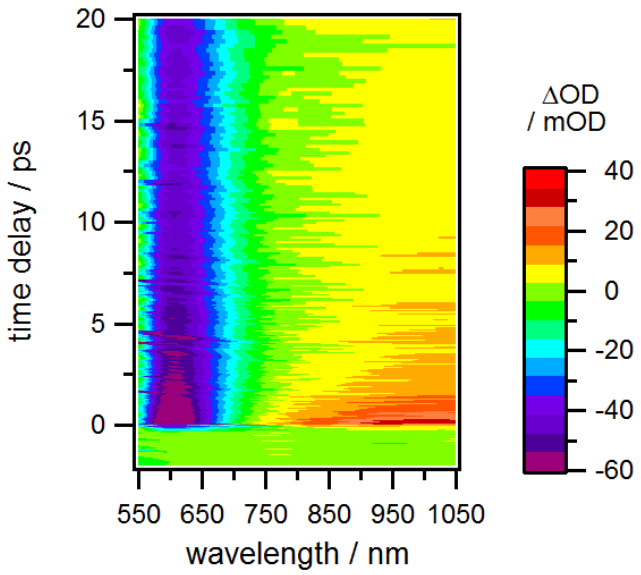

Figure 2. TA spectrum of CIS/ZnS QDs over the first 20 ps after excitation at 540 nm (1.2 μJ)

Besides the GSB, which results in reduced absorption following partial removal of the ground state population, a negative signal can also result from an emission process stimulated by the probe light. Such an SE signal is expected in photoluminescent samples and should in principle resemble the steady state PL spectrum. Despite the large Stokes-shift observed in CIS/ZnS QDs, the features in the absorption and the PL spectra are both broad enough to overlap significantly between 550 nm and 700 nm.

Hence, the negative TA signal in this region might be expected to contain contributions due to both SE and GSB.

Spectral Analysis

The transient data in figure 3 show the excited state evolution over the first 20 ps after excitation, at various pump wavelengths in the range 540-772 nm (a-d). Spectral profiles through the transients at ~1 ps show that the combined negative signal is red-shifted and apparently broader with increased pump wavelength (see SI (S1)). Since the GSB component is not expected to shift with pump wavelength, the observed red-shift could be related to a SE component stretching out to longer wavelengths. In fact, initial fitting done on spectral cuts at 10 ps revealed such a negative band around 700 nm (see SI (S2)). The ~1 ps spectral cut data in figure 3 were fit, using three Gaussian components: one positive, centred at 950 nm, representing ESA; and two negative, representing GSB and SE. No constraints were imposed on the GSB component. The centre position (693 nm) and FWHM (100 nm) were fixed for the SE component on the basis of the steady state PL spectrum, but no constraints were imposed on the amplitude of any of the three components. A strong positive signal at the excitation wavelength, an artefact of the incomplete subtraction of scattered excitation light, was removed manually from each profile prior to fitting.

Fitting reveals that the long wavelength component of the negative signal is centred at ~700 nm and stretches out to about 850 nm, consistent with the steady state luminescence spectrum. The second negative component is assigned to the GSB signal. The red-shift of the negative band as a function of excitation wavelength can thus be understood as a change in the relative intensity of the GSB and the SE components. The relative area of the SE component increases with pump wavelength, although the overall absorption cross-section falls rapidly (see figure 1), suggesting that saturation of the emitting state is occurring at shorter excitation wavelengths. With 772 nm excitation, direct absorption to the CB should not be energetically possible, yet a weak GSB signal is observed and the SE component remains

relatively strong. Two-photon excitation may be weakly populating the CB, which subsequently decays to the trap states with high efficiency, avoiding saturation due to the low absorption cross section.

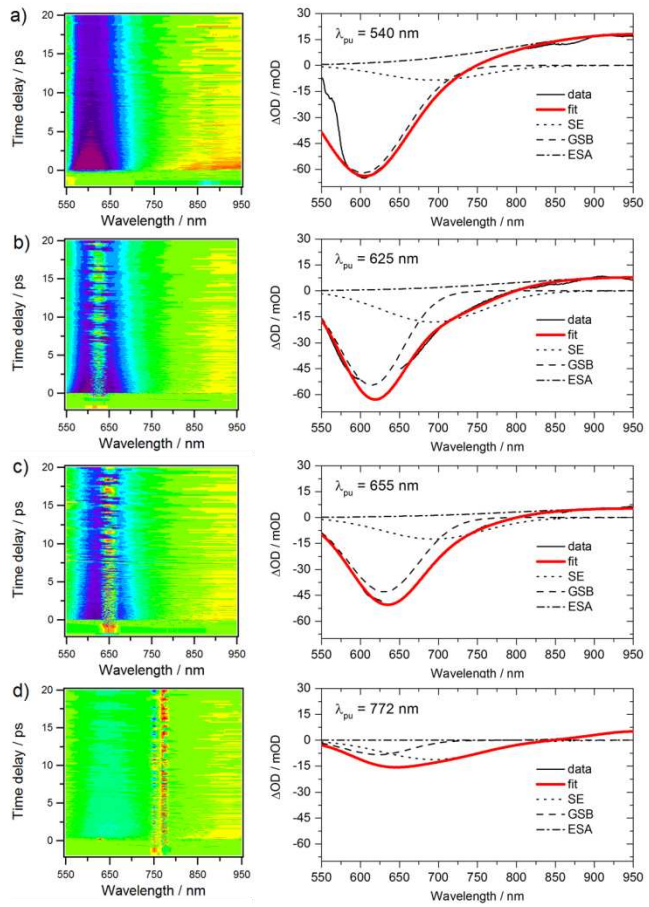

Figure 3. TA data with spectral cut (at ~1 ps) of CIS/ZnS QDs acquired with varying excitation wavelength and pump intensity. a: $\lambda = 540$ nm, 1.1 μJ; b: $\lambda = 625$ nm, 0.6 μJ; c: $\lambda = 655$ nm, 0.7 μJ; d: $\lambda = 772$nm, 4.5 μJ. TA data colour scale as in figure 2.

Kinetic Analysis

Time-zero, scattered-light corrected kinetic traces close to the GSB and ESA centre positions of 620 nm and 950 nm, respectively, are shown in figure 4. Both signals appear instantaneously within the temporal resolution of the excitation laser (~60 fs). Figure 4(b) shows the first 5 ps of the 950 nm and 620 nm data points that have been used in the initial fitting (*n.b.* the 620 nm data set and its correspond-

ing fitting function has been inverted in the normalization step for easier comparison). The 620 nm data were fit with a bi-exponential recovery function with offset (blue) and the 950 nm data with a tri-exponential decay function with offset (red). The extracted time constants for the bi-exponential recovery function at 620 nm were (27 ± 1) ps and (1.8 ± 0.1) ps.

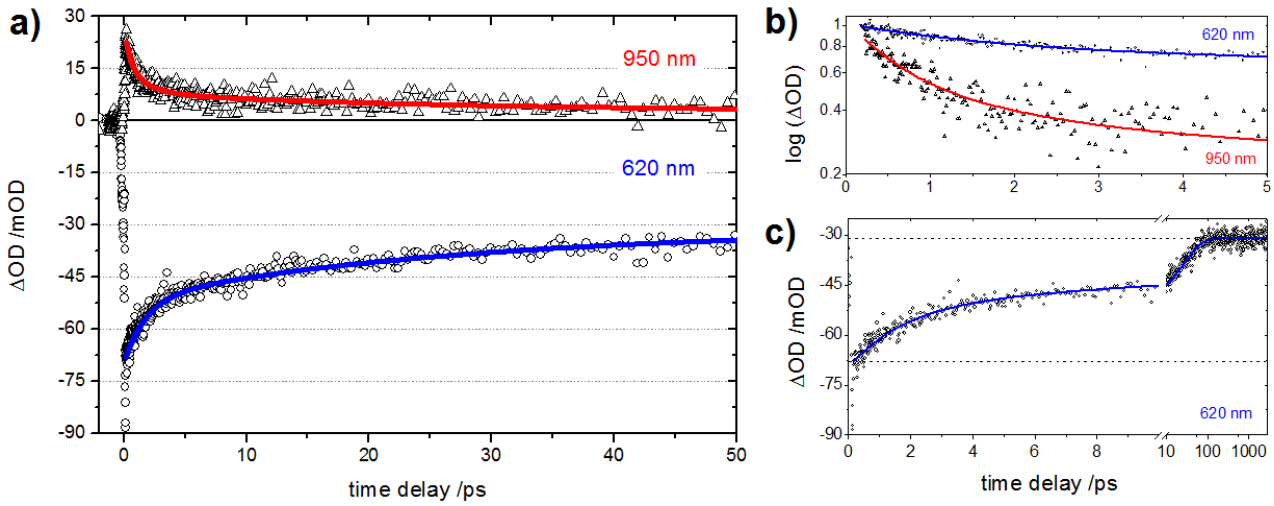

Figure 4. a: Kinetic cuts at 620 nm (circles) with the blue line representing a bi-exponential fit and at 950 nm (triangles) with the red line representing a tri-exponential fit. b: First 5 ps with normalized data points for the fitted range on a logarithmic scale (620 nm data inverted). c: Kinetics showing initial signal amplitude and final amplitude at 2.8 ns for the 620 nm data. Note break in the linear time delay axis at 10 ps to logarithmic scale.

After 2.8 ns (not shown) the transient at 620 nm levels off to an intensity of -31 mOD, which corresponds to ~45 % of the initial value at time zero. That the GSB recovery is incomplete is consistent with a fraction of excitons being trapped in the emitting state on a timescale of 10-100 ns, as previous time-resolved PL studies suggest.[15] The kinetic data at 950 nm (figure 4) were fit with the two time constants derived from the 620 nm data (*i.e.* 1.8 ps and 27 ps), but required an additional fast (0.5 ± 0.2 ps) component, which makes up 43 % of the overall signal amplitude at 950 nm, to describe the early decay as

can be seen in figure 4(b). We therefore assign this ultra-fast component that is only present in the ESA signal to a non-radiative decay into the long-lived emissive state, most likely a deep donor state arising from an internal point defect. Kinetic analysis of the data presented in figure 3(d) also indicate a growing SE signal component with τ = ~0.4 ps (at ~700 nm), which further suggests a relaxation mechanism *via* a sub-bandgap state (see SI (S5)).

A correlation between the amplitudes of the 27 ps component in the 620 nm and the 950 nm signals was observed, each making up ~30 % of the total amplitude, once the data was normalised to exclude the carriers trapped in the long-lived state. This indicates a direct coupling between the CB and VB that can be described by Auger recombination. Multi-excitation processes such as Auger effects require high pump fluence, which our experimental conditions provide; we have calculated the average occupation number of the 1s electron state, $\langle n_{1s} \rangle$, to be close to unity with at least 10 absorbed photons per particle on average (see SI (S3)). Thus, the offset in the 620 nm data could also include a contribution from Auger recombination.

The faster component of ~1.8 ps could be explained by either carrier cooling or additional carrier trapping, most likely at remaining surface defects due to incomplete surface passivation with ZnS. However, the excitation wavelength in this study is such that single-photon excitation into higher quantised states is unlikely on energetic grounds. Carrier cooling is therefore expected to be minimal and we attribute the 1.8 ps component with surface trapping. This is corroborated by a lack of characteristic derivative-shaped spectral features in the GSB (see Figure 2).

Pump-Dump-Probe Experiments

To confirm that the 0.5 ps time constant is related to the observed PL in CIS/ZnS QDs, a dump laser centred at a wavelength longer than the absorption band edge was used to drive the stimulated emission process. The TA spectrum shown in figure 5(a) was pumped at 540 nm and dumped, after 6 ps, at 772 nm. Kinetic profiles at 600 nm, 695 nm and 950 nm are shown in figure 5(b). At the dump time po-

sition, the total signal intensity at 600 nm and 695 nm are reduced to ~42 % and ~75 % relative to the previous values, respectively, whereas the ESA at 950 nm is unaffected. No spectral decomposition was performed, however the latter qualitative observation is the most interesting, as it provides direct evidence that the absorbing excited state is not depopulated by the dump laser and is therefore not the emissive state. The instant appearance of the ESA signal with the excitation laser implies it originates in the CB, whilst the delayed rise of the SE component (~0.4 ps), which fits well with the 0.5 ps time constant assigned to a decay into an intra-gap state, implies that the SE originates from a sub-bandgap state. Therefore, the traditional picture of both ESA and SE originating from the CB[34] is not consistent with the pump-dump-probe data. The TA signal in the wavelength region 750 nm to 850 nm shows a small increase in absorption, which is interpreted as a loss of the SE signal upon population dump. This observation lends support to the idea that the observed room temperature PL in CIS/ZnS QDs can be attributed to the fraction of electrons which undergo an ultra-fast, non-radiative relaxation from the CB into a long-lived, high-lying donor state. Whether the PL originates from a coupling with a low-lying acceptor state or with the valence band remains an open question. However, the instantaneous response of the GSB signal to the dump laser indicates either direct coupling to the valence band or ultrafast decay of the populated low-lying acceptor state on a sub-150 fs timescale. In either case, it is clear that the emission cannot originate from the CB edge, but rather, must involve high-lying intra-gap donor states.

Our results postulate an electron-hole recombination via a trapped electron, which is contradictory to the conclusion drawn in a recent publication by Cadirci *et. al*[35] that also investigated the relaxation dynamics with femtosecond TA spectroscopy. Cadirci *et. al*[35] point out that 'the maximum bleach should be twice the value after electron trapping', which is in good agreement with the data presented here in figure 4(c), where the bleach amplitude increases from -70 mOD to a plateau of ly -32 mOD after 50 ps. Admittedly, a direct comparison between the study by Cadirci *et. al*[35] and the work presented in this paper is difficult as experimental conditions, such as excitation wavelength and

pump fluence, are different. Nevertheless, our findings are further supported by a recently published study by Omata *et. al*[20], who carried out a detailed size-dependent photoluminescence study on CIS QDs and attributed the origin of the PL emission to either indium-copper anti-site defects (In_{Cu}) and/or sulphur vacancy (V_S) defect states. It is argued that the V_S-to-V_{Cu} (copper vacancy, V_{Cu}) non-radiative coupling is the dominant recombination pathway in CIS core-only QDs as the density of V_S and V_{Cu} at the surface is high.[19] This agrees with the interpretation by Klimov *et al.* and explains the low PLQY with competitive non-radiative pathways related to surface states.[37] It is thus generally accepted that V_S trap states at the QD surface provide a very efficient de-excitation channel in CIS QDs, and that they can be suppressed by surface treatment.[19, 37-41] Based on the dramatic gain in PLQY on surface passivation, along with the observed effect of [Cu]/[In] ratio on PLQY, it is clear that V_S states at the surface are not involved in the highly radiative recombination route in fully passivated CIS/ZnS QDs. The fs-TA data reveal a minor (~3 mOD) residual ESA component, even after 2.8 ns (see figure 4). The insensitivity of this signal to the dump laser precludes the emitting trap states as an origin of this signal.

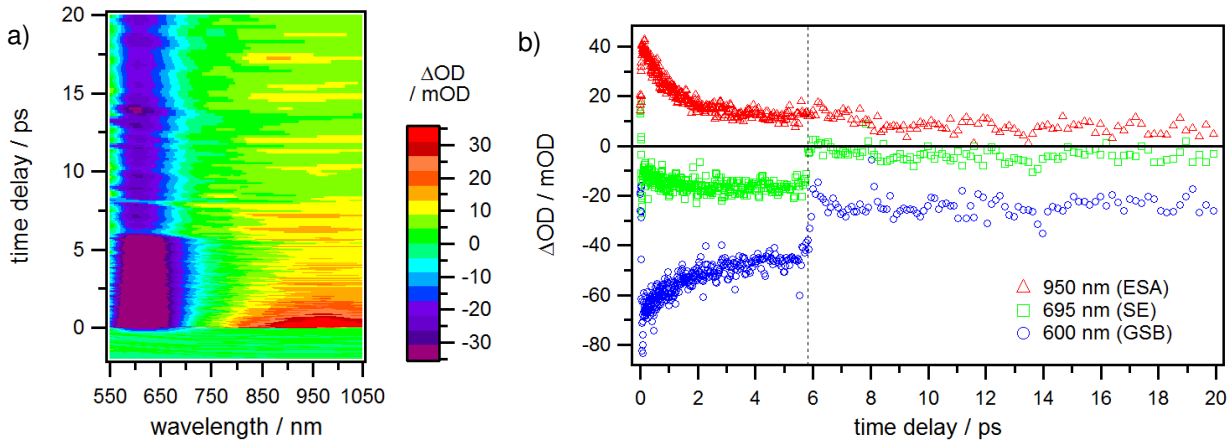

Figure 5. TA spectrum of CIS/ZnS QDs (a) dumped at 772 nm, after 6 ps. The kinetics (b) are analysed at the GSB (blue dots, SE (green squares) and ESA (red triangles) spectral fitting positions, resulting from the analysis in figure 3. The temporal position of the dump pulse is indicated (dashed line).

There remain two possible origins for the long time offset in the ESA: Internal defect sites may trap a small fraction of the CB population in the interior of the QD and in the absence of efficient non-radiative decay *via* surface V_{Cu} sites, these traps may be long lived. Alternatively, the formation of a photoproduct could give rise to this offset at long time. There is some evidence in the 950 nm data (figure 5(b)) for a picosecond timescale decay of the ESA residual following the dump pulse, which might suggest refilling of the depopulated trap states. However, the effect is weak and our data are not conclusive in this regard. Furthermore, this effect would not occur under weaker illumination as would typically be present in relevant applications.

Based on studies of the similar semiconductor $CuInSe_2$ the neutral defect complexes [In_{Cu}^{2+} + $2V_{Cu}^{+}$] and [Cu_{In}^{2-} + In_{Cu}^{2+}] can be expected to have relatively low formation energies in CIS, especially in the copper-poor phase.[8] Furthermore, the formation of [Cu_{In}^{2-} + In_{Cu}^{2+}] anti-site dimers is promoted in the vicinity of [In_{Cu}^{2+} + $2V_{Cu}^{+}$] defects, and large defect 'clusters' tend to be formed around sulfur anions, especially in nanocomposite CIS.[42] The identification of In_{Cu} or Cu_{In} defects as being involved in the highly radiative recombination process is therefore consistent with observations of the effects of off-stoichiometry on the PLQY.[28] From μs-TA studies in the bulk it is known that the In_{Cu} state is an effective trap state (~20 μs)[31] that can emit to the valence band, as can Cu_{In} states.

Nam *et al.* have previously discounted both DAP recombination and transitions directly into the valence band (VB) on the grounds that the dependency on QD size of the VB and intra-gap states cannot account for the size dependence of the observed PL spectrum. They therefore conclude that CB emission must be involved in the radiative transition.[19] However, the extent to which the individual VB, CB and intra-gap state energies depend on QD size is not well known. Cyclic voltammetry studies performed on CIS QDs of various sizes indicate that the CB and VB actually shift much more evenly than predicted from confinement models that are based on the effective-mass approximation.[10, 26] We therefore propose

a model of the relaxation dynamics of CIS/ZnS QDs involving emission from deep In_{Cu} trap states, as shown in figure 6.

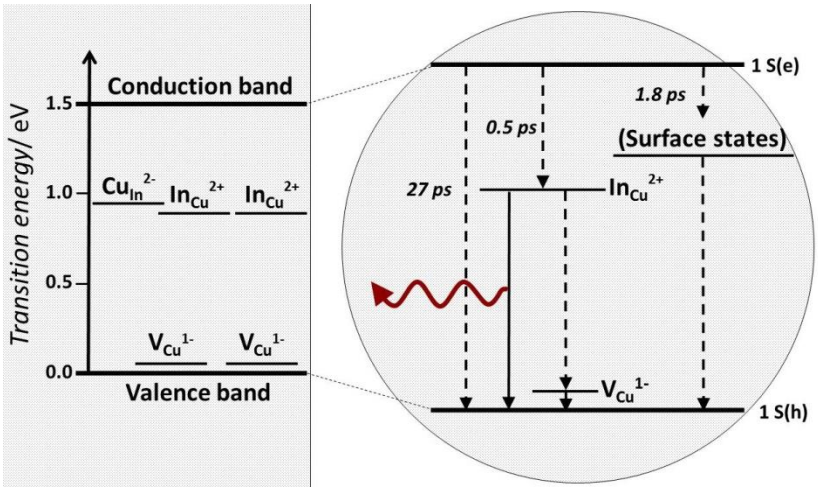

Figure 6. Illustration of the proposed recombination pathways involving the intra-gap defect complexes [Cu_{In}^{2-} + In_{Cu}^{2+}] and [In_{Cu}^{2+} + $2V_{Cu}^{+}$] in bulk CIS (left) and quantum-confined CIS/ZnS QDs (right). Solid lines represent proposed radiative transitions and dashed lines represent non-radiative transitions.

In figure 6, the defect states are represented by their reported positions (in bulk CIS) relative to the valence band maximum,[9] which is taken as the zero-energy level, although the shifts in energy shown in figure 6 for the CIS QDs are estimated. The observed PL maximum at 693 nm corresponds to 1.79 eV, which appears to be consistent with a donor state to VB transition. The corresponding Stokes shift of ~0.5 eV (based on a band gap of ~2.3 eV) is consistent with the expected relative positions of In_{Cu} or Cu_{In} defects to the CB, assuming such deep trap states move only weakly with the CB energy as the particle size is reduced.

It is known that the electronic structure of ternary chalcopyrite compounds, in particular the hybridized *p* and *d* orbitals near the VB edge, leads to an increased VB energy in bulk CIS. As the QD dimensions are reduced, the energetic overlap and thus exchange integrals between the S 4*p* and Cu 3*d* orbitals will be reduced due to confinement. Therefore, the extent of *p*-*d* hybridization can be expected to be re-

duced, lowering the VB energy and increasing the observed band gap.[43, 44], Similar effects have been demonstrated in copper-doped CdSe QDs[45] and HgTe nanoparticles.[46]

Our model of In_{Cu}-VB emission in CIS QDs, based on our femtosecond dump data, is therefore consistent with theoretical models of size dependence in ternary chalcopyrite systems, once hybridization effects are considered.

Conclusion

Steady state spectroscopy performed on CIS QDs indicates the involvement of intra-gap states in the photoluminescence process, consistent with studies on CIS in thin film and bulk.[29-32, 47] In this study transient absorption (TA) spectroscopy was performed on CIS/ZnS QDs, revealing two time constants (27 ps and 1.8 ps) in the recovery of the negative component. We identify the 27 ps time constant as Auger recombination and the 1.8 ps time constant as population flow into a surface defect state. A third time constant (0.5 ps) observed only in the infra-red excited state absorption (ESA) signal is related to a non-radiative decay into an internal defect state.

A dump laser was used to depopulate the upper state of the radiative transition. Significantly, the excited state absorption at long wavelengths was unaffected by the dump pulse, confirming that the radiative transition does not involve the conduction band as previously proposed by others,[15, 19, 34, 35] but one of the high-lying donor states. This clarification highlights the ability of standard fs-TA spectroscopy, modified by the inclusion of a third dump laser, to control carrier populations. This enables extended insight into excited state dynamics, as we show here.

Based on recent literature discussing the enhanced PLQY of CIS/ZnS QDs and copper-deficient CIS QDs compared to stoichiometric CIS QDs, together with the time constant assignment in this work, we assign the indium-copper anti site as being the origin of the observed photoluminescence. The anomalous Stokes-shift and broad non-band-edge emission in CIS and CIS/ZnS QDs are explained by this

model. The results presented in this work may be of potential importance to charge extraction in CIS QDs sensitised solar cells and to the optimisation of the PLQY for biological imaging applications.

AUTHOR INFORMATION

Corresponding Author

* Tel.: +44 (0) 113 343 3873, E-mail: k.critchley@leeds.ac.uk

Author Contributions

All authors have given approval to the final version of the manuscript.

Funding Sources

This work was financially supported by the BHRC (University of Leeds), EPSRC, and the Royal Society.

ACKNOWLEDGMENT

The authors would like to thank S.D. Evans for useful discussions.

ASSOCIATED CONTENT

Supporting Information Available: Spectral peak shift (S1) and details related to initial spectral fitting (S2); calculation of average occupation number (S3); and magnification of TA data set and kinetics (S4). This material is available free of charge *via* the Internet at http://pubs.acs.org.

ABBREVIATIONS

CB, conduction band; CIS, $CuInS_2$; CIS QDs, $CuInS_2$ quantum dots; CIS/ZnS QDs, $CuInS_2$/ZnS core/shell quantum dots; Cu_i, interstitial coppers; DAP, donor-acceptor pair; ESA, excited state absorption; fs-TA, femtosecond transient absorption; FWHM, full-width half maximum; GSB, ground state bleach; In_{Cu}, indium-copper anti-site; ΔOD, change in optical density, PDP, pump-dump-probe; PL,

1 photoluminescence; PLQY, photoluminescence quantum yield; SE, stimulated emission; VB, valence

2 band; V_{Cu}, copper vacancy; V_S, sulfur vacancy.

3

REFERENCES

(1) Shay, J. L.; Kasper, H. M. Direct Observation of Cu *d* Levels in I-III-VI_2 Compounds. *Phys. Rev. Lett.* **1972**, 29, 1162-1164.

(2) Shay, J. L.; Tell, B. Energy Band Structure of I–III–VI_2 Semiconductors. *Surf. Sci.* **1973**, 37, 748-762.

(3) Shay, J. L.; Tell, B.; Kasper, H. M.; Schiavone, L. M. Electronic Structure of $AgInSe_2$ and $CuInSe_2$. *Phys. Rev. B: Condens. Matter Mater. Phys.* **1973**, 7, 4485-4490.

(4) Ueng, H. Y.; Hwang, H. L. The Defect Structure of $CuInS_2$. Part I: Intrinsic Defects. *J. Phys. Chem. Solids* **1989**, 50, 1297-1305.

(5) Jaffe, J. E.; Zunger, A. Theory of the Band-Gap Anomaly in ABC_2 Chalcopyrite Semiconductors. *Phys. Rev. B: Condens. Matter Mater. Phys.* **1984**, 29, 1882-1906.

(6) Noufi, R.; Axton, R.; Herrington, C.; Deb, S. K. Electronic Properties versus Composition of Thin Films of $CuInSe_2$. *Appl. Phys. Lett.* **1984**, 45, 668-670.

(7) Vidal, J.; Botti, S.; Olsson, P.; Guillemoles, J. F.; Reining, L. Strong Interplay between Structure and Electronic Properties in $CuIn(S,Se)_2$: A First-Principles Study. *Phys. Rev. Lett.* **2010**, 104, 056401.

(8) Huang, D.; Persson, C. Stability of the Bandgap in Cu-Poor $CuInSe_2$. *J. Phys.: Condens. Matter* **2012**, 24, 455503.

(9) Chen, H.; Wang, C.-Y.; Wang, J.-T.; Hu, X.-P.; Zhou, S.-X. First-Principles Study of Point Defects in Solar Cell Semiconductor $CuInS_2$. *J. Appl. Phys.* **2012**, 112, 084513.

(10) Omata, T.; Nose, K.; Otsuka-Yao-Matsuo, S. Size Dependent Optical Band Gap of Ternary I-III-VI_2 Semiconductor Nanocrystals. *J. Appl. Phys.* **2009**, 105, 073106-5.

(11) Aldakov, D.; Lefrancois, A.; Reiss, P. Ternary and Quaternary Metal Chalcogenide Nanocrystals: Synthesis, Properties and Applications. *J. Mater. Chem. C* **2013**, 1, 3756-3776.

(12) Zhong, H.; Bai, Z.; Zou, B. Tuning the Luminescence Properties of Colloidal I–III–VI Semiconductor Nanocrystals for Optoelectronics and Biotechnology Applications. *J. Phys. Chem. Lett.* **2012**, 3, 3167-3175.

(13) Pons, T.; Pic, E.; Lequeux, N.; Cassette, E.; Bezdetnaya, L.; Guillemin, F.; Marchal, F.; Dubertret, B. Cadmium-Free $CuInS_2$/ZnS Quantum Dots for Sentinel Lymph Node Imaging with Reduced Toxicity. *Acs Nano* **2010**, 4, 2531-2538.

(14) Yong, K. T.; Roy, I.; Hu, R.; Ding, H.; Cai, H.; Zhu, J.; Zhang, X.; Bergey, E. J.; Prasad, P. N. Synthesis of Ternary $CuInS_2$/ZnS Quantum Dot Bioconjugates and their Applications for Targeted Cancer Bioimaging. *Integr. Biol.* **2010**, 2, 121-129.

(15) Li, L.; Pandey, A.; Werder, D. J.; Khanal, B. P.; Pietryga, J. M.; Klimov, V. I. Efficient Synthesis of Highly Luminescent Copper Indium Sulfide-Based Core/Shell Nanocrystals with Surprisingly Long-Lived Emission. *J. Am. Chem. Soc.* **2011**, 133, 1176-1179.

(16) Hines, M. A.; Guyot-Sionnest, P. Synthesis and Characterization of Strongly Luminescing ZnS-Capped CdSe Nanocrystals. *J. Phys. Chem.* **1996**, 100, 468-471.

(17) Dabbousi, B. O.; Rodriguez-Viejo, J.; Mikulec, F. V.; Heine, J. R.; Mattoussi, H.; Ober, R.; Jensen, K. F.; Bawendi, M. G. (CdSe)ZnS Core−Shell Quantum Dots: Synthesis and Characterization of a Size Series of Highly Luminescent Nanocrystallites. *J. Phys. Chem. B* **1997**, 101, 9463-9475.

(18) Jones, M.; Lo, S. S.; Scholes, G. D. Quantitative Modeling of the Role of Surface Traps in CdSe/CdS/ZnS Nanocrystal Photoluminescence Decay Dynamics. *Proc. Natl. Acad. Sci. Unit. States Am.* **2009**, 106, 3011-3016.

(19) Nam, D. E.; Song, W. S.; Yang, H. Noninjection, One-Pot Synthesis of Cu-Deficient $CuInS_2$/ZnS Core/Shell Quantum Dots and their Fluorescent Properties. *J. Colloid Interface Sci.* **2011**, 361, 491-496.

(20) Omata, T.; Nose, K.; Kurimoto, K.; Kita, M. Electronic Transition Responsible for Size-Dependent Photoluminescence of Colloidal $CuInS_2$ Quantum Dots. *J. Mater. Chem. C* **2014**, 2, 6867-6872.
(21) Park, J.; Kim, S.-W. $CuInS_2$/ZnS Core/Shell Quantum Dots by Cation Exchange and their Blue-Shifted Photoluminescence. *J. Mater. Chem.* **2011**, 21, 3745-3750.
(22) Zhong, H. Z.; Zhou, Y.; Ye, M. F.; He, Y. J.; Ye, J. P.; He, C.; Yang, C. H.; Li, Y. F. Controlled Synthesis and Optical Properties of Colloidal Ternary Chalcogenide $CuInS_2$ Nanocrystals. *Chem. Mater.* **2008**, 20, 6434-6443.
(23) Li, L.; Daou, T. J.; Texier, I.; Tran, T. K. C.; Nguyen, Q. L.; Reiss, P. Highly Luminescent $CuInS_2$/ZnS Core/Shell Nanocrystals: Cadmium-Free Quantum Dots for In Vivo Imaging. *Chem. Mater.* **2009**, 21, 2422-2429.
(24) Kuo, K. T.; Chen, S. Y.; Cheng, B. M.; Lin, C. C. Synthesis and Characterization of Highly Luminescent $CuInS_2$ and $CuInS_2$/ZnS (Core/Shell) Nanocrystals. *Thin Solid Films* **2008**, 517, 1257-1261.
(25) Tran, T. K. C.; Le, Q. P.; Nguyen, Q. L.; Li, L.; Reiss, P. Time-Resolved Photoluminescence Study of $CuInS_2$/ZnS Nanocrystals. *Adv. Nat. Sci: Nanosci. Nanotechnol.* **2010**, 1, 025007.
(26) Zhong, H.; Lo, S. S.; Mirkovic, T.; Li, Y.; Ding, Y.; Li, Y.; Scholes, G. D. Noninjection Gram-Scale Synthesis of Monodisperse Pyramidal $CuInS_2$ Nanocrystals and their Size-Dependent Properties. *Acs Nano* **2010**, 4, 5253-5262.
(27) Uehara, M.; Watanabe, K.; Tajiri, Y.; Nakamura, H.; Maeda, H. Synthesis of $CuInS_2$ Fluorescent Nanocrystals and Enhancement of Fluorescence by Controlling Crystal Defect. *J. Chem. Phys.* **2008**, 129, 134709.
(28) Chen, B. K.; Zhong, H. Z.; Zhang, W. Q.; Tan, Z. A.; Li, Y. F.; Yu, C. R.; Zhai, T. Y.; Bando, Y. S.; Yang, S. Y.; Zou, B. S. Highly Emissive and Color-Tunable $CuInS_2$-Based Colloidal Semiconductor Nanocrystals: Off-Stoichiometry Effects and Improved Electroluminescence Performance. *Adv. Funct. Mater.* **2012**, 22, 2081-2088.
(29) Krustok, J.; Schön, J. H.; Collan, H.; Yakushev, M.; Mädasson, J.; Bucher, E. Origin of the Deep Center Photoluminescence in $CuGaSe_2$ and $CuInS_2$ Crystals. *J. Appl. Phys.* **1999**, 86, 364-369.
(30) Castro, S. L.; Bailey, S. G.; Raffaelle, R. P.; Banger, K. K.; Hepp, A. F. Synthesis and Characterization of Colloidal $CuInS_2$ Nanoparticles from a Molecular Single-Source Precursor. *J. Phys. Chem. B* **2004**, 108, 12429-12435.
(31) Goossens, A.; Hofhuis, J. Spray-Deposited $CuInS_2$ Solar Cells. *Nanotechnology* **2008**, 19, 424018.
(32) Hofhuis, J.; Schoonman, J.; Goossens, A. Elucidation of the Excited-State Dynamics in $CuInS_2$ Thin Films. *J. Phys. Chem. C* **2008**, 112, 15052-15059.
(33) Komarala, V. K.; Xie, C.; Wang, Y.; Xu, J.; Xiao, M. Time-Resolved Photoluminescence Properties of $CuInS_2$/ZnS Nanocrystals: Influence of Intrinsic Defects and External Impurities. *J. Appl. Phys.* **2012**, 111, 124314.
(34) Sun, J.; Zhu, D.; Zhao, J.; Ikezawa, M.; Wang, X.; Masumoto, Y. Ultrafast Carrier Dynamics in $CuInS_2$ Quantum Dots. *Appl. Phys. Lett.* **2014**, 104, 023118.
(35) Cadirci, M.; Masala, O.; Pickett, N.; Binks, D. Ultrafast Charge Dynamics in $CuInS_2$ Nanocrystal Quantum Dots. *Chem. Phys.* **2014**, 438, 60-65.
(36) Booth, M.; Brown, A. P.; Evans, S. D.; Critchley, K. Determining the Concentration of $CuInS_2$ Quantum Dots from the Size-Dependent Molar Extinction Coefficient. *Chem. Mater.* **2012**, 24, 2064-2070.
(37) Klimov, V. I.; Mikhailovsky, A. A.; McBranch, D. W.; Leatherdale, C. A.; Bawendi, M. G. Quantization of Multiparticle Auger Rates in Semiconductor Quantum Dots. *Science* **2000**, 287, 1011-1013.

(38) Tyagi, P.; Kambhampati, P. False Multiple Exciton Recombination and Multiple Exciton Generation Signals in Semiconductor Quantum Dots Arise from Surface Charge Trapping. *J. Chem. Phys.* **2011**, 134, 094706-10.
(39) Kim, Y.-K.; Ahn, S.-H.; Chung, K.; Cho, Y.-S.; Choi, C.-J. The Photoluminescence of $CuInS_2$ Nanocrystals: Effect of Non-Stoichiometry and Surface Modification. *J. Mater. Chem.* **2012**, 22, 1516-1520.
(40) Sewall, S. L.; Cooney, R. R.; Anderson, K. E. H.; Dias, E. A.; Sagar, D. M.; Kambhampati, P. State-Resolved Studies of Biexcitons and Surface Trapping Dynamics in Semiconductor Quantum Dots. *J. Chem. Phys.* **2008**, 129, 084701.
(41) Klimov, V. I. Optical Nonlinearities and Ultrafast Carrier Dynamics in Semiconductor Nanocrystals. *J. Phys. Chem. B* **2000**, 104, 6112-6123.
(42) Nanu, M.; Boulch, F.; Schoonman, J.; Goossens, A. Deep-Level Transient Spectroscopy of TiO_2/$CuInS_2$ Heterojunctions. *Appl. Phys. Lett.* **2005**, 87, 242103.
(43) Yoodee, K.; Woolley, J. C.; Sa-yakanit, V. Effects of *p-d* Hybridization on the Valence Band of I-III-VI_2 Chalcopyrite Semiconductors. *Phys. Rev. B: Condens. Matter Mater. Phys.* **1984**, 30, 5904-5915.
(44) Hsu, T. M. *p-d* Hybridization of the Valence Bands of Copper Indium Disulfide. *J. Appl. Phys.* **1991**, 69, 3772-3774.
(45) Wright, J. T.; Meulenberg, R. W. Modification of the Conduction Band Edge Energy *via* Hybridization in Quantum Dots. *Appl. Phys. Lett.* **2012**, 101, 193104.
(46) Rath, S.; Sahu, S. N. Electronic Structure of HgTe Nanocrystals: An Observation of *p–d* Weakening. *Surface Science* **2006**, 600, L110-L115.
(47) Liu, X. H.; Dou, X. M.; Sugiyama, M. Photoluminescence Studies in $CuInS_2$ Thin Films Grown by Sulfurization Using Ditertiarybutylsulfide. *J. Appl. Phys.* **2012**, 112, 123521.
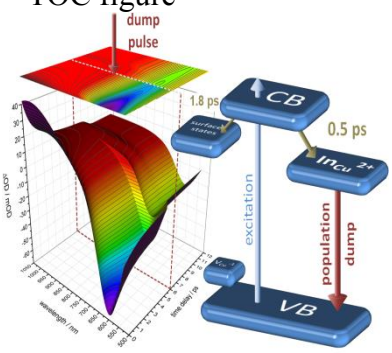
TOC figure